The DOI for this manuscript is doi: 10.1175/BAMS-D-13-00262.1

Global Precipitation Measurement Cold Season Precipitation Experiment (GCPEx): For Measurement Sake Let it Snow

Author List: Gail Skofronick-Jackson[1], David Hudak[2], Walter Petersen[3], Stephen W. Nesbitt[4], V. Chandrasekar[5], Stephen Durden[6], Kirstin J. Gleicher[4], Gwo-Jong Huang[5], Paul Joe[7], Pavlos Kollias[8], Kimberly A. Reed[4], Mathew R. Schwaller[1], Ronald Stewart[9], Simone Tanelli[6], Ali Tokay[10], James R Wang[11], Mengistu Wolde[12]

[1]NASA Goddard, Greenbelt, MD
[2]Environment Canada, King City, ON, Canada
[3]NASA Wallops Flight Facility, Wallops Island, VA
[4]University of Illinois at Urbana-Champaign, Urbana, IL
[5]Colorado State University, Fort Collins, CO
[6]Jet Propulsion Laboratory, Pasadena, CA
[7]Environment Canada, Toronto, ON, Canada
[8]McGill University, Montreal, PQ, Canada
[9]University of Manitoba, Winnipeg, MB, Canada
[10]JCET, University of Maryland Baltimore County, Baltimore, MD
[11]Science Applications International Corporation
[12]National Research Council of Canada, Ottawa, ON, Canada

Corresponding Author: Gail Skofronick-Jackson
NASA Goddard Space Flight Center
Code 612, 8800 Greenbelt Rd, Greenbelt, MD 20771 USA
Gail.S.Jackson@nasa.gov
301-614-5720

Submitted to BAMS June 11, 2014

Revised October 27, 2014

Abstract—250 words max

As a component of the Earth's hydrologic cycle, and especially at higher latitudes, falling snow creates snowpack accumulation that in turn provides a large proportion of the fresh water resources required by many communities throughout the world. To assess the relationships between remotely sensed snow measurements with *in situ* measurements, a winter field project, termed the Global Precipitation Measurement (GPM) mission Cold Season Precipitation Experiment (GCPEx), was carried out in the winter of 2011-2012 in Ontario, Canada. Its goal was to provide information on the precipitation microphysics and processes associated with cold season precipitation to support GPM snowfall retrieval algorithms that make use of a dual-frequency precipitation radar and a passive microwave imager onboard the GPM core satellite, and radiometers on constellation member satellites. Multi-parameter methods are required to be able to relate changes in the microphysical character of the snow to measureable parameters from which precipitation detection and estimation can be based. The data collection strategy was coordinated, stacked, high-altitude and *in situ* cloud aircraft missions with three research aircraft sampling within a broader surface network of five ground sites taking *in-situ* and volumetric observations. During the field campaign 25 events were identified and classified according to their varied precipitation type, synoptic context, and precipitation amount. Herein, the GCPEx field campaign is described and three illustrative cases detailed.

Capsule: 20-30 words: *In-situ* and remotely-sensed observations of falling snow with coordinated ground and aircraft measurements reveal the microphysical and radiative parameters of snow.

Background and Motivation

Precipitation falling in the form of snow is critically important for society, climate, geology, agriculture, and ecosystems. Falling snow can exert tremendous socio-economic impacts and disrupt transportation systems. Snowpacks store freshwater and reflect incoming radiant energy. Indeed, in some parts of the world including the U.S., snow is the dominant precipitation type and relied upon year round for freshwater. Despite the importance to human activity and understanding of the Earth's system, measuring falling and fallen snow remains a challenge (e.g., Kulie et al. 2010, Lohnert et al. 2011, Derksen et al. 2012, Foster et al. 2012).

It is difficult to obtain global and fully representative measurements of both rain and snow with ground based instruments. Ground instruments are sparse (especially over water bodies), require automated data logging 24 hours a day/7 days a week, and are beset with challenges due to the inherent spatial and temporal variability of precipitation (Nitu et al. 2012, Rasmussen et al. 2003, Rasmussen et al. 2012). For falling snow, ground instrument measurements (e.g., Joe et al. 2014, Huang et al. 2009, Battaglia et al. 2010, Saavedra et al. 2011, Sheppard and Joe 2008) can be very problematic because snowflakes have many shapes and densities that affect their fall speed, fall trajectories, and volume-to-melted water ratios.

Ice-phase precipitation detection and retrieval algorithms using satellite passive radiometer observations have been reported and shown to be useful in studying near-surface falling snow (Skofronick-Jackson et al. 2004; Ferraro et al. 2005; Chen and Staelin 2003; Noh et al. 2009). The passive millimeter-wave and sub-millimeter-wave frequencies are especially sensitive both to the scattering and absorption/emission properties of atmospheric ice particles and these channels have been exploited in the above approaches. In addition to passive radiometer retrievals of snow from space, Wood (2011), Liu 2008, and Kulie and Bennartz (2009) have developed algorithms to retrieve snowfall properties and their uncertainties using the W-band reflectivity measurements and ancillary data from CloudSat. It is reasonable to suggest that a combined active-passive approach should reduce the uncertainties in snow estimation.

Accordingly, the Global Precipitation Measurement (GPM) mission, with its core satellite launched February 27, 2014, has been designed to provide calibrated and uniform active and passive precipitation (rain and falling snow) measurements over the majority of the globe at a temporal resolution of 2-4 h (Hou et al. 2014). The GPM core observatory satellite is specifically designed to estimate rain rates from 0.2 to 110 mm/h and to detect falling snow (Hou et al., 2014). Other theoretical studies have shown that GPM can be expected to be able to detect and estimate falling snow liquid water equivalents above ~0.5 mm/hr melted (Skofronick-Jackson et al., 2013, Munchak and Skofronick-Jackson 2013).

PLACE SIDEBAR 1 HERE

While early results from the GPM spacecraft indicate that the retrieval algorithms are obtaining falling snow estimates, physically-based snowfall retrieval algorithms for GPM are in an active phase of development. Further refinement and testing of these emerging algorithms requires the collection of targeted high-quality ground-validation datasets in snowing environments. The GPM Cold Season Precipitation Experiment (GCPEx), a collaboration between the NASA GPM Ground Validation (GV) program and its international partner Environment Canada (EC) provided both new datasets and physical insights related to the snowfall process to ultimately improve falling snow retrievals.

The GCPEx field campaign occurred in Ontario, Canada (Fig. 1) from January 15, 2012 to March 3, 2012. GCPEx collected microphysical properties, associated remote sensing observations, and coordinated model simulations of precipitating snow (hereafter “falling snow” and/or “snowfall” will be used interchangeably in reference to precipitating snow). GCPEx expands upon the successful Canadian CloudSat/CALIPSO Validation Programme (C3VP) held the winter of 2006-2007 (Hudak et al. 2006, Barker et al. 2008). While successful, C3VP lacked additional surface stations to examine subgrid variability, did not include the high altitude satellite remote sensing proxy for GPM, nor did it have such a carefully orchestrated set of measurements.

The primary objective of GCPEx was to conduct a complete study of snowfall physical properties and radiative properties from the ground through the atmospheric column as would be measured by GPM spacecraft. GCPEx measurements addressed significant areas of weakness or knowledge gaps in snowfall detection and estimation algorithms including: (1) lack of realistic representation of snow particles, their bulk density, size and shape distributions, and their associated radiative properties in forward radiative transfer models that convert physical properties to radiative properties; (2) limited physically-based means to assess the behavior and mitigation of highly variable surface emissivities on satellite passive microwave (PMW) measurements over multiple temporal scales and surface types, (3) the low sensitivity to light/moderate falling snow events by passive sensors, and (4) ambiguities in reflectivity-snow rate (Ze-S) and brightness temperature-ice water path (TB-IWP) relationships. GCPEx provided information used to characterize the ability of multi-frequency active and passive microwave sensors to detect and estimate falling snow. It also addresses the capability of validating the relationships between snow’s physical properties and its radiative properties.

PLACE SIDEBAR 2 HERE

The “Design of the Experiment” section provides information on the field campaign measurements, locations, instruments and sampling strategies. In the “Measured Cases” section a summary of the field campaign observations is supplied from beginning to end. The section on “Experimental Highlights” details the aircraft and ground based falling snow measurements for three interesting cases for GCPEx. The “Data Management” section provides data access information while “Summary and Outlook” is a look forward toward GCPEx data usage.

Design of Experiment

The coordinated measurement strategy used stacked high-altitude GPM airborne remote sensing simulator instrumentation and *in-situ* cloud aircraft flights with three research aircraft sampling within a broader network of five ground sites taking surface *in-situ* and volumetric observations (Fig. 1). The observing framework used a combination of multi-frequency radar, particle imaging and water equivalent-measuring surface instrumentation in conjunction with airborne dual-frequency radar, high frequency radiometer and *in situ* microphysics observations to provide the most complete coupled 3D sampling of surface and in-cloud microphysical properties possible. To focus instruments on high impact observations that can be used pre- and post-launch for retrievals, the GPM algorithm developers identified key measurements needed to constrain algorithm assumptions (Table 1 and sidebar 2). These parameters link to instruments and sensors at the ground, *in situ*, and remotely sensed by high altitude aircraft (Table 2).

Ground Measurement Instrumentation and Strategy

Ground sampling was focused about a densely-instrumented central location, the Environment Canada (EC) Centre for Atmospheric Research Experiments (CARE) at 44° 13’ 57" N / 79° 46’ 53" W. CARE is well situated within both mid-latitude synoptic and lake-effect snowfall regimes and under the coverage of the EC C-band dual polarization scanning radar located at King City (green circles in Fig. 1). All ground instrumentation (Table 3) was designed to operate 24/7 or be switched on during snow events. The active remote sensing instrumentation suite at CARE included multi-frequency, dual polarized Doppler radars, lidars, and wind profilers. The passive remote sensing suite included multiple several channel radiometers. *In-situ* measurements at CARE included a multiple disdrometers, various video and photographic devices and a number of other technologies that estimate instantaneous precipitation rate. In addition, a wind blocking Double Fence International Reference (Nitu et al., 2012) liquid equivalent precipitation measurement was done manually at regular intervals (Table 3).

Measurements conducted at four secondary ground sites (yellow triangles in Fig. 1 and Table 4) represented a slightly reduced observational capability to that available at the CARE site. These secondary site measurements provided a means to extend and calibrate volumetric radar products over the broader domain sampled by the King City radar (more appropriate to the scale of satellite footprints of 5-25 km). They also allow opportunities to connect airborne measurements to locations at the ground other than the CARE Facility and to sample lake effect events that tend to be localized and spatially fine-scale in nature. Table 3 provides references and a summary of the ground-based equipment deployment at the primary CARE site and at the secondary sites.

Aircraft Measurement, Instrumentation and Strategy

For airborne sampling the DC-8 aircraft served as a GPM satellite simulator, carrying the Conically-Scanning Millimeter-wave Imaging Radiometer (CoSMIR) with passive channels spanning 50[1]-183 GHz and the Airborne Second Generation Precipitation Radar (APR-2), with a Ku and Ka-band radar. The University of North Dakota (UND) Citation and the National Research Council (NRC) Convair-580 hosted *in situ* microphysics sensors and provided information on the vertical distribution of cloud and snow microphysical properties. Details on the aircraft instrumentation and references are found in Table 5. Flight legs were aligned along a range height indictor (RHI) scan axis of the King City radar and/or in coordinated stacked profiling spirals (Citation, Convair), or in orbiting patterns (DC-8) above the heavily instrumented primary/secondary ground sites. Aircraft flights occurred during precipitation events, with the exception of two DC-8 missions designed to measure brightness temperatures associated with land surface emission during intervening cloud-free periods.

The DC-8 aircraft was selected for the GCPEx due to its compatibility with the desired instrument payload, its altitude ceiling (~12.5 km) and its ability to fly long duration missions (e.g., 10 h based the GCPEx payload). The DC-8 was based out of Bangor, Maine with an approximate flight time to the CARE site of one hour. The Citation and Convair aircraft sampled the column of snow/ice from ~800 m AGL to 7000 m AGL. The Citation and Convair were based out of Muskoka and Ottawa, respectively (Fig. 1) and were flown consecutively during the longer duration DC-8 flights. Convair participation in the experiment was limited to February 2012.

The weather forecasting process was an integral part of the planning for aircraft missions. The lead time required to deploy the DC-8 from its staging location in Maine required significance advanced planning. The forecasting duties were divided between students from the

[1] The 50 GHz channels on COSMIR are not on the GPM spacecraft but remain as part of heritage channels of CoSMIR.

U. of Illinois and McGill University. The forecasting teams had access to Numerical Weather Prediction (NWP) model output from both EC and the US National Weather Service (NWS). To leverage local forecasting expertise, the forecasting teams also consulted on a daily basis with EC operational forecasters.

Measured Cases

The totality of the surface, ground based remote sensing, aircraft and satellite data resulted in a comprehensive 3D volume/column of data providing a description of snowfall physics at the ground and through the atmospheric column, and also a database of scenes for evaluating and developing satellite snowfall retrieval algorithms. Data collected during this field campaign exceeded all expectations, with measurements of heavy (>50 mm hr^{-1} fluffy, *non-melted*, rate), moderate (25 – 50 mm h^{-1}), and light falling snow rates, along with mixed phase and rain cases. These heavy through light snow cases are ideal for testing the thresholds of detection for falling snow rates using GPM-like sensors.

The project was conducted from January 15, 2012 until March 3, 2012. However, much of the ground instrumentation was installed during November 2011. As a result, many sensors obtained additional data from the early part of the winter. In total, 25 events were identified (Table 6). An event was determined subjectively as a period of contiguous or nearly contiguous precipitation that corresponded to a specific synoptic triggering mechanism. The event total SWE amounts were the manual measurements taken by the Tretyakov gauge inside the Double Fence International Reference (DFIR) wind shield at CARE. The precipitation type was characterized as rain (R), snow (S), or mixed precipitation that could include ice pellets (R/S). The synoptic context was determined from the daily synopsis produced by the project weather forecasters. The final categories were frontal disturbances (F), low pressure passages but without a surface frontal passage (C), an upper air feature not reflected in a distinct surface low (U), a lake effect event from flows off either Lake Huron or Georgian Bay (L), or a ridge (Ri). The final columns identify which events had specific aircraft involvement.

The precipitation measurements at CARE were made using a Pluvio 400 precipitation weighing gauge, a Pluvio 200 weighing gauge (heated rim), and the manual DFIR reference measurement (Nitu et al. 2012). The data are either liquid precipitation amount when raining or snow water equivalent (SWE) amounts when snowing. The manual measurements have a coarser time resolution, typically 12 h, compared to the Pluvio gauge that has a resolution of one minute. On an event basis (falling snow water equivalent amounts > 1 mm), the correlation between the Pluvio 400 and the manual reference gauge is 0.96 with ~ -1% mean bias. This is in keeping with Rasmussen et al. (2012) and lends confidence to the use of the Pluvio 400 gauge as the reference precipitation amount at the 5 surface sites. The time series of precipitation accumulation at the CARE site is shown in Figure 2a. There was a total of 103 mm of liquid equivalent precipitation during the six-week project, 100 mm of which fell during organized events. Event periods with aircraft sampling are superimposed on Fig. 2a with vertical color bars. The research aircraft were involved in 18 of the 25 events. Fig. 2b gives the measured distribution of precipitation rates averaged over 10 min during the project. Approximately 70% of the measured rates were < 2.0 mm h^{-1}.

As an example of the variability of precipitation structure, Fig. 3a gives the area-wide precipitation accumulation for the 30 January event based on radar reflectivity using the C-band King City radar. The coefficients in the Ze-S algorithm were derived from an analysis of the 2DVD measurements at all the ground sites as outlined in Huang et al. (2014). The pattern illustrates the complexity of the precipitation and the influence of the open water to the northwest on lake-enhancement of the precipitation. Fig. 3b shows the time history of accumulation for the radar and the Pluvio 400 measurements at Huronia to the north. At the range of Huronia the radar beam is at an altitude of ~ 1 km. For the first 8 h, the correspondence of the radar derived amounts and the Pluvio gauge was excellent, allowing for a 15 min temporal offset due to the low fall velocity of snow. Thereafter the radar derived amount was considerably less than the measured amount. This was during a period when the lake-enhancement was the most significant and low-level echo growth below 1 km in altitude was typical. A comparison of the radar reflectivity with the POSS, a small bistatic X-band radar measuring precipitation close to the ground (Sheppard and Joe 2008) confirmed this increase in reflectivity below 1 km.

While the focus of DC-8 airborne operations was primarily oriented to sampling falling snow, an effort was also made to collect measurements of land surface emission characteristics during cloud-free days of the experiment (events 9 and 18 in Table 6). Here the focus was on collection of CoSMIR radiometer views of the land surface under the influence of varying snow and vegetation conditions in order to understand and possibly mitigate the influence of land-surface emission properties on passive radiometer snowfall retrieval algorithms. In at least one case, clear air and snowing cases were sampled along the same flight line on two adjacent days. Accompanying observations from excavated snow pits and ground-based downward looking radiometer observations of the snowpack were conducted at the CARE site in support of this activity.

Precipitation in general, and snowfall in particular, were below normal during the winter of 2011-12. Early in the project, any significant precipitation amounts invariably involved either rain or mixed precipitation. The middle part of the experiment had generally light snowfall events or lake effect events captured by aircraft but not directly over the main measurement site at CARE. However, the latter part of the experiment saw a number of significant snowfall events with liquid equivalent rates up to 5 mm h^{-1} as measured at the CARE site.

Experiment Highlights

Three of the important and diverse systems sampled during the GCPEx field campaign were events 6, 8, and 21. Event 6 occurred on 27 January 2012 and was a mixed phase event that produced 14.2 mm of liquid equivalent precipitation. This event produced freezing rain and snow near CARE within a wraparound region of a cyclone that tracked through the eastern Great Lakes. Event 8 on 30-31 January 2012 was a light snow system with measurements of 3.5 mm of Snow Water Equivalent (SWE) at the CARE site and was driven by an upper air feature. Event 20 on 24 February 2012 was a major cyclone giving a snowfall total of 8.3 mm SWE at CARE.

Event 6: 27 January 2012

Event 6 (27 January 2012) featured near-surface radar reflectivities exceeding 30 dBZ over the southern part of the experimental domain associated with near-surface mixed phase and liquid precipitation near 2:30 UTC (Fig 4a). A radiosonde launched at CARE at 2353 UTC 26 January 2012 (not shown) indicated a layer above freezing between 780 and 895 hPa, with a layer as cold as –4°C below this warm layer indicating the possibility of mixed surface precipitation. Ice pellets, snow, and freezing rain were observed, and icing was severe enough to cause hazardous road conditions near the CARE site. The DC-8 and Citation sampled these bands of moderate precipitation in excellent coordination with flight legs parallel to radar Range Height Indicator (RHI) scans along a line from the King City 331° azimuth through and beyond CARE. All radar data indicates a strong melting layer near 1.5 km with radar echoes extending to above 5 km on both the ground based King City and D3R (Dual-frequency, Dual-polarimetric Doppler Radar) radars (not shown) as well as the APR-2 aboard the DC-8 (Fig. 4b), and the echo structure above the melting level had the appearance of upright convection. Above the melting layer, D3R (not shown) and APR-2 (Fig. 4c) observed Ku-Ka dual frequency ratio (DFR) values exceeding 7 dB indicating non-Rayleigh scattering. Within the melting layer, the D3R indicated higher DFR values (> 14 dB), which suggests particle orientation and differential path attenuation were likely playing a role in the differing DFR values based on viewing angle (not shown). In the rain, DFR values were lower than aloft, but still non-zero (values of 2-3 dB from APR-2) indicating the presence of rain drops with median mass diameters of 1.5-2 mm. Within this event, it is likely that the GPM Dual-frequency Precipitation Radar (DPR) would capture a large portion of the surface precipitation with both its Ku and Ka band radar (nominal minimum detectable signals of 17 and 12 dBZ, respectively).

Within this mixed phase precipitation event, CoSMIR nadir-viewing passive microwave signatures (Fig. 4d) were complex, and appeared to respond to the vertical structure of the sampled system in the channels with frequencies < 183 GHz. The background surface brightness temperature contribution was low due to pre-existing snow cover and cold surface temperatures (the microwave surface emissivity of snow is 0.6 to 0.7), and increases in brightness temperature associated with heavier precipitation at 89 GHz may be associated with supercooled water emission in the column. The 166 GHz channel responded to a mixture of ice scattering and emission at mid-cloud layers. The 183 GHz channels only respond to relatively deep (tall) clouds in the presence of significant water vapor, and in this case the lack of response showed that the signal is only due to water vapor emission. The CoSMIR 89 GHz conically scanning polarization difference (see Wang et al. 2013 for the polarization difference formula) was nearly 8 K between the two cores, indicating the presence of oriented ice crystals in this region.

The UND Citation spiral (Figure 5) occurred between 2:28 and 3:43 UTC measured *in situ* properties between 1 and 4.4 km MSL. It sampled one of the convective elements displayed in Figure 4. The Nevzorov total water probe (Fig. 5a) sampled total water contents in excess of 0.3 g m^{-3} near 5 km MSL, and the King liquid water probe (Fig. 5b) sampled supercooled water in excess of 0.25 g m^{-3} at these altitudes. As the aircraft descended on a 10 km diameter spiral, Fig. 5c shows the plane periodically entered and exited a region with high concentrations of large particles > 1 cm according to the 2D probes, where the median volume diameter (D_0) was in excess of 2-4 mm. Intermittently above the freezing level (located at 1.5 km MSL), the 2D probes sampled regions of small D_0 that were collocated with regions of measurable supercooled liquid water content according to the King probe. Below the melting level, small D_0 is again noted with the collapse of particle sizes associated with melting. The University of Manitoba particle study indicated rain and melting particles on the ground that melted too quickly to photograph.

Event 8: 30-31 January 2012

To contrast the mixed precipitation Event 6, a nearly identical data sampling strategy was employed in Event 8 (30-31 January 2012), and a similar analysis of data is shown from the 30-31 January snow event in Figure 6. As mentioned above, this event produced light snowfall accumulations (< 3.5 mm in 8 hours) over the sampled region, and the King City C-Band radar reflectivity image near 0:31 UTC (Fig. 6a) shows that reflectivities were generally in the 10-20 dBZ range, which would be marginally detectable by the GPM DPR. The vertical cross section (Fig. 6b) from the APR-2 radar shows very consistent reflectivity values, and an echo top between 7 and 8 km MSL. Values measured by APR-2 on the DC8 (Fig. 6c), show near zero values of DFR in most of the region except within the highest measured reflectivities where DFR approaches 4-5 dB. These low DFR values indicate that snow particle median diameters are small (~1-3 mm).

In Fig. 6d, CoSMIR brightness temperature observations for the 30-31 January light snow case reveal distinct contrasts to the 27 January freezing rain case. First, 89V brightness temperatures are more dominated by strong scattering by snow particles, with minimum values near 220 K. However, there are interesting deviations where the scattering signature is reduced and brightness temperatures increase notably at 89H, and 165 GHz. At 183 GHz, both channels do not detect any precipitation signal. Polarization differences at 89 GHz also show variability, with a peak in polarization difference of only 4.5 K near the minimum in 89 GHz brightness temperatures, indicating a possibility of oriented ice particles. Results discussed in Skofronick-Jackson et al. (2013) and Munchak and Skofronick-Jackson (2013), suggest that this event would not be easily detected by the GPM radiometer.

In Figure 7, a microphysical analysis is shown for the 30-31 January case near 23:30 UTC 30 January. Here, the precipitation was more horizontally uniform than for the 27 January case, so the values are more consistent along the spiral flight track. Note that despite lower total water contents (~0.15 g m^{-3} maximum) as measured by the Nevzorov probe (Fig. 7a), there was also significant liquid water content observed below 2.5 km MSL by the King probe (Fig. 7b, nearly ~0.15 g m^{-3} maximum). The vertical profile of particle size distributions (Fig. 7c) displayed consistent values of D_0 near 1.5-2 mm, with maximum values just below the region of supercooled water indicating possible particle growth by riming and/or vapor deposition. Also evident is a bimodal size distribution with a high concentration of particles < 0.5 mm as well as a second peak near the values of D_0 extending to maximum sizes of about 8 mm. Overall, the size distribution parameters measured with the aircraft at the minimum operating altitude and with the Parsivel-2 disdrometer on the surface at the CARE site agreed remarkably well (not shown), which demonstrates the relatively slow vertical evolution and small horizontal inhomogeneity of the particle size distribution. For this case, generally small particles were observed at the surface, and the University of Manitoba particle study indicated relatively small dendritic particles (with some aggregates) as well as irregular particles (Figure 8).

Event 20: 24 February 2012

In contrast to the January 30-31 event, a stronger, longer-duration event was observed on February 24, 2012 (event 20). Sampling during this event ranged from multi-aircraft *in-situ* microphysical data collections (back-to-back Citation, Convair, Citation flights) coordinated with the DC-8 in light to heavy snow, to single aircraft DC-8 sampling of both heavy snow and mixed phase precipitation along, over, and to the north of Lake Ontario. Collectively, the February 24 event will provide a case study to examine GPM algorithm detectability thresholds across a spectrum of snowfall intensities (i.e., light, moderate and heavy snow events).

Figure 9 shows the NOAA National Mosaic Quantitative precipitation estimates (NMQ) ground radar composite along with DC-8 aircraft measurements from the APR-2's Ku-Band radar reflectivity, dual-frequency ratio at Ku-Ka band, and CoSMIR TB and polarization differences. The radar images show intense Z values near 25 dBZ indicating heavy snow up to altitudes of 5-6 km. The CoSMIR cross-tracked scans report TB depressions of nearly 100 K for all channels except 183+/-3 due to the scattering of snow in the profile. Indeed, GMI data to date has shown 100K depressions in areas of deep convection even with the larger footprints as compared to CoSMIR. In contrast to the prior two cases, here the convection was deep enough to allow appreciable signals from ice scattering in the 183+/-3 and 183+/-7 GHz channels, with a stronger signal in the latter channel that extends further from the water vapor absorption line. In particular, the convective element sampled near hour 16.63 and 16.70 UTC, which had APR-2 Ku-Band reflectivity > 15 dBZ over 5-6 km MSL elicits a scattering response in all channels, including 183+/-3 GHz. Polarization differences (Wang et al, 2013) were not necessarily correlated with the reflectivities implying that the frozen particles may have been more spherical and/or randomly oriented instead of preferentially oriented. Further analysis of the Citation and Convair microphysical measurements during these cases will provide an excellent variety of snowfall intensities to understand the variations of microwave properties of snowfall.

Data Management

Data quality control and archiving of the GCPEX dataset has been completed. These data are most easily accessed on the GPM Ground Validation Data Portal for GCPEX http://gpm.nsstc.nasa.gov/gcpex/. This web site contains links to the datasets, instrument tables and other miscellaneous information.

From the "Data" tab off the GCPEx data portal, access to a table of case dates and quick look images from the Precipitation Video Imager(s) is provided and can be perused to assist in selection of datasets for download. From the GCPEX data site, individual components of the GCPEx dataset can be searched using the Global Hydrology Resource Center (GHRC) HyDRO tool, or the user can download an entire dataset type (radar, gauge, disdrometer etc.) directly from the data site using file transfer protocol (ftp). Documentation of daily forecasts and mission operations summaries provided by campaign Mission Scientists are available via the GCPEx

Operations Portal. Access to the Operations portal and GPCEx logs contained therein, requires a username and password obtained through the GCPEx Operations Portal.

Summary and Outlook

The GCPEx collected a unique and valuable data set. The dataset consists of 25 events during the 6 week field project consisting of 3 mixed precipitation events; 2 rain events; 18 snow events and 2 clear air calibration events. Aircraft sampling coordination during the experiment was excellent. There were 6 events sampled with 2 aircraft, and 3 events with 3 aircraft. In all, the DC-8 flew fourteen, UND Citation ten, and the Convair-580 six missions, respectively. The data collection strategy was designed to sample the column above a typical satellite pixel. Data to address shortcomings in GPM precipitation algorithms have been collected. Also, the information serves as a testbed for the development of ground radar dual polarization-based precipitation type and rate algorithms (Schuur et al. 2012). The United States NEXRAD radar network is completely dual polarized and the Canadian radar network has its dual polarization upgrade well underway. These radars are essential in network validation that is part of the GPM GV program.

Events 6, 8, and 20 detailed herein illustrate the challenges in snowfall estimation by radar, be it ground-based or space-based. Not surprisingly, the relationship between radar reflectivity and snowfall rate is non-unique as shown in Figs 4, 6, 9 where reflectivities and TBs are under constrained for different snow cases. Multi-parameter (dual frequency, dual polarization, etc.) methods are required to be able to relate changes in the microphysical character of the snow to measureable parameters from which precipitation estimates can be based. For GPM, these include algorithms that rely on dual frequency radar measurements, multi-frequency passive radiometer observations, or a combination of radar and radiometer measurements. The analysis of GCPEx data is to be carried out in way that allows developers to test the assumptions inherent in the algorithms. The data are also portrayed in a manner that allows for uncertainty estimates in the algorithm to be meaningfully derived.

It is anticipated that the GCPEX dataset will satisfy the majority of GPM falling snow retrieval algorithm validation objectives originally set forward for the experiment. These 3D datasets are suitable for conducting observational and modeling-based studies of bulk/particle scale snow microphysical and scattering properties observed at the ground, through the atmospheric column, and at high altitudes as observed from the vantage point of remote sensing instrumentation deployed on the GPM Core Observatory. Collectively a strong emphasis is placed on characterizing GPM falling snow algorithm detectability limits for both the GPM DPR and GPM Microwave Imager (GMI) instruments as related to cloud physical processes, intervening cloud environment parameters, and land surface properties. Since GPM wasn't in orbit at the time of this field campaign one cannot directly compare GPM snow retrievals to the measurements made during GCPEx. However, the field campaign did establish the usefulness of the Pluvio gauges as a validating tool and future comparisons against the satellite products over a range of falling snow rates using these gauges is now possible. The signatures of light snow rates in reflectivities and brightness temperature in events 6 and 20 (27 January 2012 and 24 February 2012) were favorably evaluated against snow rate thresholds of detection as compared to theoretical studies (Skofronick-Jackson et al, 2013, Munchak and Skofronick-Jackson, 2013). Post-launch GPM algorithm refinement and snowfall validation work is currently underway; just months after GPM's launch. In addition, during the winter of 2015-2016 GPM will conduct a field campaign in the Olympic Mountain range to measure both rain and snow.

Acknowledgments: The GPM Flight Project funded airborne and ground based instrument deployments for the NASA component of GCPEx (Ramesh Kakar and Steven Neeck). A portion of this research (Tanelli and Durden) was carried out at the Jet Propulsion Laboratory, California Institute of Technology, under a contract with the National Aeronautics and Space Administration. Portions of the research (Petersen, Tokay, Huang, Nesbitt) were also supported by NASA Precipitation Measurement Mission Science (Ramesh Kakar). Environment Canada is gratefully acknowledged for its funding support of Canadian ground based platforms and its outstanding support for managing the deployment logistics of GCPEx. Funds for the Convair C-580 were provided by CSA and NRC with in-kind contributions from EC and NASA Glenn. The authors gratefully acknowledge the contribution of Alexei Korolev of Environment Canada to the analysis of the Convair-580 data, Mike Poellot, Dave Delene, and Andrea Neuman for the 1-D Citation probe analysis, Andrew Heymsfield and Aaron Bansemer of NCAR for the 2-D Citation probe analysis, Chris Derksen for the CARE snowfall event totals, and of Larry Bliven of NASA to the PVI analysis. The Natural Sciences and Engineering Research Council of Canada assisted in supporting the particle photography measurements by Stephen Berg and Neil Fogg. The involvement of Matthew Bastian of National Research Council in the Convair-580 operations, as well as the financial support of the Canadian Space Agency, are also acknowledged.

Sidebar 1: Passive-active measurements of precipitation.

Spaceborne precipitation retrievals typically take the form of passive microwave radiometer retrievals (using brightness temperatures and polarizations at various frequencies), radar (active) retrievals, or combined retrievals, which use both radiometer and radar data. In the passive microwave, liquid hydrometeors (rain, cloud water) emit microwave radiation into the field of view, particularly at low frequencies (<40 GHz), whereas ice (snow, cloud, graupel, hail) scatters the Earth's microwave radiation out of the downlooking sensor's field of view, especially at high frequencies (>40 GHz). The amount of scattering and the polarization of the wave as viewed by the radiometer depend on the number, size, shape, and degree of melting of the hydrometeors. In addition, the emission of microwave radiation by the surface, which is highly variable over land, depends on the surface type (and surface snow can appear similar to falling snow at several passive microwave channels). These hydrometeor and surface passive microwave characteristics are strongly wavelength- and polarization-dependent. At radar wavelengths available to satellite-based radars, attenuation (absorption) and non-Rayleigh scattering by relatively large particles (compared to the wavelength), complex-shaped ice hydrometeors and snow aggregates, and melting particles are not well-characterized at present. The combination of the Rayleigh scattering at Ku-band and non-Rayleigh scattering at Ka-band leads to a difference in reflectivity termed *dual frequency ratio* (DFR). DFR from radars such as the GPM DPR can be exploited to retrieve characteristics of the particle size distribution if the scattering properties of the precipitation are known. Radar and radiometer data collected by satellite simulator aircraft in GPM field campaigns, in concert with *in situ* bulk water and ice as well as particle imaging measurements on the ground and on microphysics aircraft, will help characterize the microwave properties of hydrometeors and the surface for the validation of falling snow retrievals.

Sidebar 2: GCPEx field campaign measurements can help answer:

- What is the minimum snow rate that can be detected from spaceborne instruments under various snow and surface characteristics?

- How well can these sensors discriminate falling snow from rain or clear air?
- Can the relationships between the physical properties of falling snow and its radiative properties be parameterized?
- What are the sources of variability and error in falling snow *in situ* measurements and remotely sensed retrievals?

Acronym List

ADMIRARI	Advanced Microwave Radiometer for Rain Identification
AGL	Above Ground Level
AMSR-E	Advanced Microwave Scanning Radiometer for Earth Observing System
APR-2	Airborne Second Generation Precipitation Radar
C	Surface frontal passage events
CALIPSO	Cloud-Aerosol Lidar and Infrared Pathfinder Satellite Observations
CARE	Centre for Atmospheric Research Experiments
C/CIP	Cloud Imaging Probe
CCN	Cloud Condensation Nuclei
CCP	Cloud Combination Probe
CDP	Cloud Droplet spectra
CN	Condensation Nuclei
CORALNET	The Canadian Observational Research Aerosol Lidar Network
CoReH2O	Cold Regions Hydrology high-resolution Observatory
CPI	Cloud Particle Imager
CPSD	Cloud Particle Spectrometer with Depolarization
CRM/LSM	Cloud Resolving Model/Land Surface Model
CoSMIR	Conically-Scanning Millimeterwave Imaging Radiometer
CSA	Canadian Space Agency
CW	Cloud Water Content
C3VP	Canadian CloudSat/CALIPSO Validation Programme
2DC	2 Dimensional optical array probe
dB	Decibels
dBZ	Radar reflectivity in units of dB
DFIR	Double Fence International Reference
DFR	Dual Frequency Ratio
DPR	Dual-frequency Precipitation Radar
DSD	Drop Size Distribution
D3R	Dual-frequency dual-polarized Doppler Radar
EC	Environment Canada
ε/σ_{sfc}	Surface emission and/or backscatter cross section
F	Frontal low disturbance events

FSSP	Forward Scattering Spectrometer Probe
4D	Four-dimensional
GCPEx	Global Precipitation Measurement mission Cold Season Precipitation Experiment
GHRC	Global Hydrology Resource Center
GHz	Gigahertz
GMI	GPM Microwave Imager
GPM	Global Precipitation Measurement
GV	Ground Validation
HVPS	High-Volume Particle Spectrometer
HyDRO	Hydrology
IW	Ice Water Content
JCET	Joint Center for Earth Systems Technology
L	Lake Huron/Georgian Bay events
LDR	Linear Depolarization Ratio
LWE	Liquid Water Equivalent
MHz	Megahertz
MRR	Micro Rain Radar
MSL	Mean Sea Level
NASA	National Aeronautics and Space Administration
NAWX	NRC Airborne W and X-band radar
NCAR	National Center for Atmospheric Research
NEXRAD	Next-Generation Radar
NMQ	National Mosaic Quantitative precipitation estimates
NOAA	National Oceanic and Atmospheric Administration
NRC	National Research Council
NWS	National Weather Service
NWP	Numerical Weather Prediction
OAP-2G-P	Optical Array Probe 2 Dimensional Gray scale Precipitation
OTT	Parsivel manufacturer (www.ott.com)
Φ_{DP}	Differential Propagation phase
PARSIVEL	Particle Size and Velocity [OTT Laser optical disdrometer]
PID	Particle IDentification
PMS	Particle Measurement Systems (company)
PMW	Passive MicroWave measurements
POSS	Precipitation Occurrence Sensor System
PPI	Plan Position Indicator
PSD	Particle Size Distribution measured at the surface (SFC) or column (col)
PVI	Precipitation Video Imager
ρ	Density (b: bulk) or (p: particle)
Qsoil	Soil Moisture
Qv	Water Vapor
R	Rain
RH	Relative Humidity
RHI	Range Height Indicator
Ri	Ridge events

RUC	Rapid Update Cycle
S	Snow
SAR	Synthetic Aperture Radar
SWE	Snow Water Equivalent
TB	Microwave Brightness Temperature
TB-IWP	Brightness Temperature - Ice Water Path
TECO	Technical Conference on Meteorological and Environmental Instruments and Methods of Observations
TPS	Total Precipitation Sensor [TPS-3100 Hot Plate]
TWc	Total Water Content in Cloud
U	Distinct surface low events
UND	University of North Dakota
UTC	Coordinated Universal Time
V-H	Vertical – Horizontal
V_r	Radial Velocity
W	Spectral Width
WMO	World Meteorological Organization
Ze	Equivalent Radar Reflectivity
Z_{DFR}	Dual Frequency Ratio [dB] (also ZDR)
Ze-SR	Reflectivity – Snow Rate

REFERENCES

Barker, H. W., A. V. Korolev, D. R. Hudak, J. W. Strapp, K. B. Strawbridge, and M. Wolde, 2008: A comparison between CloudSat and aircraft data for a multilayer, mixed phase cloud system during the Canadian CloudSat-CALIPSO Validation Project. *J. Geophys. Res.*, **113**, D00A16, doi:10.1029/2008JD009971.

Battaglia, A., E. Rustemeier, A. Tokay, U. Blahak, and C. Simmer, 2010: PARSIVEL snow observations: A critical assessment. *J. Atmos. Oceanic Technol.*, **27**, 333–344, doi: 10.1175/2009JTECHA1332.1.

Boodoo, S., D. Hudak, N. Donaldson, and M. Leduc, 2010: Application of Dual-Polarization Radar Melting-Layer Detection Algorithm. *J. Appl. Meteor. Climatol.*, **49**, 1779-1793, doi:10.1175/2010JAMC2421.1

Chandrasekar, V., M. Schwaller, M. Vega, J. Carswell, K. V. Mishra, A. Steinberg, C. Nguyen, M. Le, F. Junyent and J. George, 2012: Dual-frequency dual-polarized Doppler radar (D3R) system for GPM ground validation: Update and recent field observations. *IEEE International Geoscience and Remote Sensing Symposium*, *July 22-27 2012*, Munich, Germany, 346-349, doi:10.1109/IGARSS.2012.6351567.

Chen F. W. and D. H. Staelin, 2003, AIRS/AMSU/HSB precipitation estimates. *IEEE Trans. Geosci. Remote Sens.*, **41**, 410-417, doi:10.1109/TGRS.2002.808322.

Derksen, C., P. Toose, J. Lemmetyinen, J. Pulliainen, A.Langlois, N. Rutter and M. Fuller, 2012: Evaluation of passive microwave brightness temperature simulations and snow water equivalent retrievals through a winter season. *Remote Sensing of Environment*, **117**: 236–248, doi:10.1016/j.rse.2011.09.021.

Ferraro R. R., F. Weng, N. C. Grody, L. Zhao, H. Meng, C. Kongoli, P. Pellegrino, S. Qiu, and C. Dean, 2005: NOAA operational hydrological products derived from the advanced microwave sounding unit. *IEEE Trans. Geosci. Remote Sens.*, **43**, 1036-1049, doi:10.1109/TGRS.2004.843249.

Foster, J. L., and Coauthors, 2012: Passive microwave remote sensing of the historic February 2010 snowstorms in the Middle Atlantic region of the USA. *Hydrol. Process*., **26**, 3459–3471, doi:10.1002/hyp.8418.

Hocking, W. K., M. C. Kelley, R. Rogers, W. O. J. Brown, D. Moorcroft and J.-P. St. Maurice, 2001: Resolute Bay VHF radar: A multi-purpose tool for studies of tropospheric motions, middle atmosphere dynamics, meteor physics and ionospheric physics. *Radio Sci.*, **36**, 1839-1857, doi:10.1029/2000RS001005.

Hou, A. Y., R. K. Kakar, S. Neeck, A. A. Azarbarzin, C. D. Kummerow, M. Kojima, R. Oki, K. Nakamura, T. Iguchi, 2014: The Global Precipitation Measurement (GPM) Mission. *Bull. Amer. Meteor. Soc.*, **95**, 701-722, doi:10.1175/BAMS-D-13-00164.1.

Huang, G.-J., V. N. Bringi, R. Cifelli, D. Hudak, and W. A. Petersen, 2010: A Methodology to Derive Radar Reflectivity-Liquid Equivalent Snow Rate Relations Using C-Band Radar and a 2D Video Disdrometer. *J. Atmos. Oceanic Technol*., **27,** 637-651, doi:10.1175/2009JTECHA1284.1.

Huang, G.-J., V. N. Bringi, D. Moisseev, W. A. Petersen, L. Bliven, and D. Hudak, 2014: Use of 2D-Video Disdrometer to Derive Mean Density-Size and Ze-SR Relations: Four Snow Cases from the Light Precipitation Validation Experiment. *Atmos. Res*., **153**, 34-48, doi:10.1016/j.atmosres.2014.07.013.

Hudak, D., H. Barker, P. Rodriguez, and D. Donovan, 2006: . *4th European Conf. on Radar in Hydrology and Meteorology*, Barcelona, Spain, 18-22 Sept., 2006, 609-612.

Hudak, D., W.A. Petersen, G. Skofronick-Jackson, and M. Schwaller, 2011: GCPEX Science Plan: http://pmm.nasa.gov/resources/documents/GPM.

Kneifel, S., and Coauthors, 2011: Observation of snowfall with a low-power FM-CW K-band radar (Micro Rain Radar). *Meteorol. Atmos. Physics*, **113**, 75-87, doi:10.1007/s00703-011-0142-z.

Kulie, M. S. and R. Bennartz, 2009: Utilizing Spaceborne Radars to Retrieve Dry Snowfall. *J. Appl. Meteor. Climatol.*, **48**, 2564–2580, doi: 10.1175/2009JAMC2193.1

Kulie, M.S. R. Bennartz, T. J. Greenwald, Y. Chen, and F. Weng, 2010: Uncertainties in Microwave Properties of Frozen Precipitation: Implications for Remote Sensing and Data Assimilation. *J. Atmos. Sci.*, **67**, 3471–3487. doi: http://dx.doi.org/10.1175/2010JAS3520.1

Joe, P. and Coauthors, 2014: The Monitoring Network of the Vancouver 2010 Olympics. *Pure and Applied Geophysics*, **171**(1-2), 25-58, doi:10.1007/s00024-012-0588-z.

Liu, G. 2008: A Database of Microwave Single-Scattering Properties for Nonspherical Ice Particles. *Bull. Amer. Meteor. Soc.*, **89**, 1563–1570. doi: http://dx.doi.org/10.1175/2008BAMS2486.1

Löhnert, U., S. Kneifel, A. Battaglia, M. Hagen, L. Hirsch, and S. Crewell, 2011: Toward a better understanding of snowfall microphysics: The TOSCA Project. *Bull. Amer. Meteor. Soc.*, **92**, 613-628, doi:10.1175/2010BAMS2909.1.

Munchak, S. J. and G. Skofronick-Jackson, 2013: Evaluation of precipitation detection over various surfaces from passive microwave imagers and sounders. *Atmos. Res.*, **131**, 81-94, doi: 10.1016/j.atmosres.2012.10.011.

Newman, A., P. Kucera and L. Bliven, 2009: Presenting the Snowflake Video Imager (SVI). *J. Atmos. Oceanic Technol.*, **26**, 167-179, doi:10.1175/2008JTECHA1148.1.

Nitu, R., R. and Coauthors, 2012: WMO Inter-comparison of Instruments and Methods for the Measure of Solid Precipitation and Snow on the Ground: Organization of the Experiment, WMO Technical Conference on Meteorological and Environmental Instruments and Methods of Observations (TECO-2012), Brussels, Belgium, 16-18 October 2012, http://www.wmo.int/pages/prog/www/IMOP/publications/IOM-109_TECO 2012/Session1/O1_01_Nitu_SPICE.pdf.

Noh, Y.-J., G. Liu, A. S. Jones, and T. H. Vonder Haar, 2009: Toward snowfall retrieval over land by combining satellite and in situ measurements, *J. Geophys. Res.*, **114,** D24, 27, doi:10.1029/2009JD012307.

Rasmussen, R. M., J. Hallett, R. Purcell, S. D. Landolt, and J. Cole, 2011: The Hotplate precipitation gauge. *J. Atmos. Oceanic Technol.*, **28**, 148-164, doi:10.1175/2010JTECHA1375.1.

Rasmussen, R., and Coauthors, 2012: How Well Are We Measuring Snow: The NOAA/FAA/NCAR Winter Precipitation Test Bed. *Bull. Amer. Meteor. Soc.*, **93**, 811–829, doi:10.1175/BAMS-D-11-00052.1.

Rasmussen, R., M. Dixon, S. Vasiloff, F. Hage, S. Knight, J. Vivekanandan, and M. Xu, 2003: Snow Nowcasting Using a Real-Time Correlation of Radar Reflectivity with Snow Gauge

Accumulation. *J. Appl. Meteor*., **42**, 20–36, doi:10.1175/1520-0450(2003)042<0020:SNUART>2.0.CO;2.

Saavedra P., A. Battaglia and C. Simmer, 2011: Partitioning of cloud water and rain water content by ground-based observations with the Advanced Microwave Radiometer for Rain Identification (ADMIRARI) in synergy with a micro rain radar. *J. Geophys. Res*., **117**, D5, 16, doi:10.1029/2011JD016579.

Schuur, T. J., H.-S. Park, A. V. Ryzhkov, and H. D. Reeves, 2012: Classification of Precipitation Types during Transitional Winter Weather Using the RUC Model and Polarimetric Radar Retrievals. *J. Appl. Meteor. Climatol*., **51**, 763-779, doi:10.1175/JAMC-D-11-091.1.

Sheppard B. E., and P. I. Joe, 2008: Performance of the Precipitation Occurrence Sensor System as a Precipitation Gauge. *J. Atmos. Oceanic Technol*., **25,** 196-212, doi:10.1175/2007JTECHA957.1.

Skofronick-Jackson, G., M.-J. Kim, J. A. Weinman, and D. E. Chang, 2004: A physical model to determine snowfall over land by microwave radiometry. *IEEE Trans. Geosci. Remote Sens*., **42**, 1047–1058, doi:10.1109/TGRS.2004.825585.

Skofronick-Jackson, G.M.; B. T. Johnson, S. J. Munchak, 2013: Detection Thresholds of Falling Snow From Satellite-Borne Active and Passive Sensors. *IEEE Transactions on Geoscience and Remote Sensing*, **51**, 4177 - 4189, doi: 10.1109/TGRS.2012.2227763.

Strawbridge, K. B., M. G. Harwood, M. S. Travis and B. J. Firanski, 2008:. The Canadian Observational Research Aerosol Lidar Network (CORALNET). *Proc. 24th Intl Laser Radar Conf.*, June 23-27, Boulder, CO. 2008.

Tanelli, S., S. L. Durden, and E. Im, 2006: Simultaneous measurements of Ku- and Ka-band sea surface cross-sections by an airborne radar, *IEEE Geosci. Remote Sens. Lett*., **3**, 359–363, doi:10.1109/LGRS.2006.872929.

Theriault, J. M., K. L. Rasmussen, T. Fisico, R. E. Stewart, P. Joe and G. Isaac, 2012: Weather observations along Whistler Mountain during five storms. *Pure Applied Geoph.* **171**, 129-155, doi 10.1007/s00024-012-0590-5.

Tokay, A., D. B. Wolff, and W. A. Petersen, 2014: Evaluation of the new version of the laser-optical disdrometer, OTT Parsivel^2. *J. Atmos. Oceanic. Technol*., **31**, 1276-1288, doi:10.1175/JTECH-D-13-00174.1.

Wang, J. R.; G. M. Skofronick-Jackson, M. R. Schwaller, C. M. Johnson, W. B. Monosmith, Z. Zhang, 2013: Observations of Storm Signatures by the Recently Modified Conical Scanning Millimeter-Wave Imaging Radiometer. *Geoscience and Remote Sensing, IEEE Transactions on*, **51**, 411-424, doi:10.1109/TGRS.2012.2200690.

Wolde, M., & Pazmany, A. (2005, October). NRC dual-frequency airborne radar for atmospheric research. In *32nd Int. Conf. on Radar Meteor*.

Wolde, M., D. Hudak, A. V. Korolev, and J. W. Strapp, 2010: Airborne Radar Observation of A Major Winter Storm: Use of Dual-frequency and Polarimetric Measurements in Studies Cloud Structures and Processes. 13th Conference on Cloud Physics, *Amer. Meteorol. Soc.*, CD-ROM paper J4.6.

Wood, N. B., 2011: Estimation of snow microphysical properties with application to millimeter-wavelength radar retrievals for snowfall rate. Ph.D. dissertation, Colorado State University, 248 pp. [Available from Colorado State Univ., Digital Collections, http://hdl.handle.net/10217/48170].

Table 1: Retrieval components, assumptions, or issues (leftmost column) along with needed GV measurements to be used to develop and improve falling snow detection and estimation.

Algorithm component, assumptions, or issue addressed for GCPEx	Applicable Measured and/or Diagnosed Parameters																
	Z	Z_{DFR}	S	*PSD sfc*	*PSD col*	*PID*	$\square_b$	$\square_p$	T	Q_v	Q_{soil}	*CN CCN*	TW_c	*CW*	*IW*	$\square/\square_{sfc}$	T_B
Path integrated attenuation approach(es)	✐	✐	✐	✐	✐	✐				✐			✐	✐		✐	
Hydrometeor Identification (3D)	✐	✐	✐	✐	✐	✐	✐		✐				✐	✐	✐		
Bulk snow particle habit properties	✐	✐	✐	✐	✐	✐	✐	✐	✐				✐		✐		✐
Bulk snow particle size distributions	✐	✐	✐	✐	✐	✐	✐	✐	✐								✐
Detection thresholds for falling snow	✐	✐	✐	✐	✐	✐	✐	✐	✐					✐	✐	✐	✐
Dual-Frequency snow detection	✐	✐	✐	✐	✐	✐										✐	
Near surface rain estimate/rain profile	✐	✐	✐	✐	✐	✐										✐	
Sub-pixel DSD and snow variability (correlation, errors, beam filling)	✐	✐	✐	✐	✐	✐											✐
DSD profile	✐	✐	✐	✐	✐	✐											✐
Column/Land surface emission			✐						✐	✐	✐					✐	✐
Rain/snow discrimination	✐	✐	✐	✐	✐	✐			✐	✐			✐	✐	✐	✐	✐
Ice particle vs. volume extinction	✐	✐			✐	✐	✐	✐	✐	✐					✐		✐
Cloud water profiles/ice water profiles	✐	✐	✐						✐	✐		✐	✐	✐	✐		✐
Ice process, scattering, and snowfall	✐	✐	✐	✐	✐	✐	✐	✐					✐	✐	✐		✐
Regime controls on precipitation process	✐	✐	✐	✐	✐	✐	✐	✐	✐	✐		✐	✐	✐	✐	✐	✐
DSD Gamma-Triplet correlations	✐	✐	✐	✐	✐	✐							✐				
CRM/LSM Satellite Simulator Physics	✐	✐	✐	✐	✐	✐	✐	✐	✐	✐	✐	✐	✐	✐	✐	✐	✐
Land surface emission			✐						✐					✐		✐	✐
Coupling upper cloud ice processes & surface snow rates/detection	✐	✐	✐	✐	✐	✐	✐	✐	✐				✐	✐	✐		✐

Table 2: Instrumentation and measurements for GCPEx. The parameters measured link to the needs of algorithm developers indicated in Table 1.

GCPEx GV measurements			Applicable Measured and/or Diagnosed Parameters																	
	Instruments	Measurable	*Z*	*Z* *DFR*	*R*	*PSD sfc*	*PSD col*	*PID*	$\square_b$	$\square_p$	*T*	Q_v	Q_{soil}	*CN, CCN*	TW_c	*CW*	*IW*	$\square/\square_{sfc}$	T_B
Ground Radar and Profiler	C-band Dual-Pol	Z, Vr, W, ZDR, □ DP, □hv	x		x	x	x	x											
	D3R Ka/Ku Dual-Pol	Z, Vr, DFR, W, ZDR, □ DP, □hv, LDR	x	x	x	x	x	x											
	X-band profiling	Z, Vr, W	x		x			x											
	MRR2 profiling	Z, Vr, W	x		x	x	x	x											
	W-band profiling	Spectra (Z, Vr)	x		x	x	x	x								x			x
	Dual freq. LIDAR	□					x												
Ground Gauge and Radiometer	2DVD/Parsivel/POSS	DSD, shape, fall spd	x		x	x		x											
	Pluvio2 SWE Gauges	SWE Rate			x														
	TPS 3100 Hot Plate	SWE Rate, Wind, T			x						x								
	Soundings	P, T, RH, wind									x	x							
	ADMIRARI Radiometer, MRR	T_B 19, 37 Z 24 GHz	x		x											x			
	EC TP3000 Radiometer	TB 23-59 GHz									x	x				x			
	EC Ground-Staring Radiometer	TB 10-89 GHz															x		x
	EC Surface Met. Inst.	P,T,RH, wind									x	x							
Aircraft	APR2 (Ka/Ku Radar)	Z, Vr, DFR, W, LDR	x	x	x		x	x										x	
	CoSMIR (Radiometer)	T_B 50, 89, 165.5,183 H/V															x	x	x
	CPI/2D-C/CIP, HVPS	Precip. Image	x		x		x	x	x	x					x		x		
	CDP	Cloud Water/Spectra					x									x			
	Nevzorov	Total water							x						x	x	x		
	King Probe	Cloud water bulk														x			
	Rosemount Icing Probe	Supercooled water														x			
	Aircraft T/RH/Gust	Air T, RH, wind									x	x							

Table 3: A summary of the ground-based measurements, associated instrumentation and appropriate references.

Instrument	#	Purpose and (Site Distribution)	Provider; Reference
C-band Dual Pol. Radar	1	4-D Precipitation (King City)	Boodoo et al. (2010);
D3R Ka/Ku, Dual Pol Radar	1	4-D Precipitation (CARE)	NASA; Chandrasekar et al. (2012)
W-band vertically pointing	1	Cloud/hydrometeor profiles (CARE)	McGill U.; http://www.radar.mcgill.ca/facilities/vertix.html; http://www.clouds.mcgill.ca/facilities.html
X-band vertically pointing	1	Hydrometeor profiles (CARE)	McGill U.; http://www.radar.mcgill.ca/facilities/vertix.html; http://www.clouds.mcgill.ca/facilities.html
Micro Rain Radar (24.2 GHz)	5	PSD and precipitation profile (1/site)	NASA/EC; Kneifel et al. (2011)
ADMIRARI Radiometer + MRR (19-37 GHz)	1	Cloud/liquid water retrievals (CARE)	U. Bonn/Leicester; Saavedra et al. (2011)
Ground-Stare Radiometer (1.4, 19, 37, 89 GHz)	1	SWE snowpack (CARE)	Derksen (2012)
Dual Pol. Radiometer (89-150 GHz)	1	Scanning/profiling water content (CARE)	U. Cologne
2D Video Disdrometer	5	PSD/precip rate/variability (1/site)	NASA; Huang et al. (2010), Newman et al. (2009)
OTT Parsivel Disdrometer	10	PSD/precip Rate/variability (2/site)	NASA; Battaglia et al. (2010), Tokay et al. (2014)
POSS	5	PSD/precip rate (1/site, except Mortons)	Sheppard and Joe (2008)
Precipitation Video Imager	3	PSD/Image (CARE, Huronia, Steamshow)	NASA, Newman et al. (2009)
Snow Camera	1	High res. imagery (CARE)	U. Manitoba
Pluvio-2 Weighing Gauge (200, 400)	9	SWE accum/rate (~2/site)	NASA; Rasmussen et al. (2011)
TPS 3100 Hot Plate	5	SWE accum/rate (1/site)	NASA; Rasmussen et al. (2011)

Snow LWE system (L-band + sonic)	5	SWE accum/rate (~1/site)	NASA (Duke U.)
Rawinsonde (soundings)	1	T/P/RH profiles (CARE)	EC; Hudak et al. 2011
Surface Meteorology	5	T/RH/P/Winds (1/site)	http://gpm.nsstc.nasa.gov/gcpex/
High Frequency Radiometer	1	Ice Water Path (CARE)	Löhnert et al. (2011)
Dual Channel lidar	1	Cloud and Aerosol backscatter profiles (CARE)	Strawbridge et al. (2008)
Snow Particle photography	1	Precipitation particles morphology (CARE)	Theriault et al. (2012)
Ground staring radiometers, snow course mapping	1	snow depth, density, stratigraphy (CARE)	Derksen et al. 2012
Wind Profiler (50 MHz) Wind Profiler (915 MHz)	1 1	Wind profiles and turbulence Wind profiles and turbulence (CARE)	Hocking et al. (2001) EC

Table 4: A summary of the secondary site locations.

Name	Location with respect to CARE site	Latitude	Longitude
Steam Show Fairgrounds	7.8 km southeast	44°10'48.30"N	79°43'7.78"W
SkyDive Toronto	11.2 km east	44°14'14.20"N	79°38'26.96"W
"Sheltered valley" rural residence (Morton's)	12.6 km west	44°10'35.29"N	79°55'9.13"W
Huronia Airport	52 km northwest	44°41'24.26"N	79°55'51.94"W

Table 5: A summary of the aircraft platforms, their instrumentation and references.

Instrumentation	Description	Reference
NASA DC-8		
APR-2 (Active)	13.4, 35.6 GHz (H, V)	Tanelli et al. (2006)
CoSMIR (Passive) H+V	50, 89, 165.5, 183.3+/-1, 183.3+/-3, 183.3+/-7 GHz	Wang et al. (2013)
UND Citation		
Optical Array Probes: 2DC, CIP, HVPS-3, CPI, CDP	particle sizes from 2 µm to 2 cm	http://cumulus.atmos.und.edu/
State parameters	temperature, dewpoint, pressure, 3D winds	http://cumulus.atmos.und.edu/
Bulk microphysics: Nevzorov, King, Rosemount Probes	liquid water and total water content	http://cumulus.atmos.und.edu/
NRC Convair-580		
Optical Array and associated Probes: PMS 2D-C/P, FSSP, OAP-2G-P, CCP, CPSD	particle sizes from 25 µm to 6 mm	Wolde et al. (2010); http://www.nawx.nrc.gc.ca/convair.html
State parameters	temperature, dewpoint, pressure, 3D winds	http://www.nawx.nrc.gc.ca/index2.html
Bulk microphysics: Nevzorov, King, Rosemount Probes	liquid water and total water content	http://www.nawx.nrc.gc.ca/index2.html
NAWX radar	W and X-band dual polarization radar	Wolde and Pazmany, 2005

Table 6: A summary of the events during the field project. See text for an explanation. Note that the final aircraft flight hours were used during the 25 February 2012 flights and hence no flights occurred after that date.

Event No.	Start (UTC)	End (UTC)	SWE Amount (mm)	Pcpn Type	Synoptic Context	Aircraft		
						DC-8	UND	Convair
1	17/1/2012/12	18/1/2012/13	11.1	R/S	F			
2	19/1/2012/15	20/1/2012/04	1.4	S	F	x	x	
3	21/1/2012/06	21/1/2012/23	0.7	S	L	x		
4	23/1/2012/07	24/1/2012/00	4	R	C			
5	24/1/2012/04	25/1/2012/03	0.7	S	C			
6	27/1/2012/01	27/1/2012/20	14.2	R/S	C	x	x	
7	28/1/2012/13	29/1/2012/12	1.9	S	U	x	x	
8	30/1/2012/20	31/1/2012/04	3.5	S	U	x	x	
9	1/2/2012/19	2/2/2012/22	0	None	U			x
10	4/2/2012/15	4/2/2012/18	0.1	None	Ri	x		
11	7/2/2012/02	7/2/2012/12	0.4	S	L	x		
12	10/2/2012/19	11/2/2012/12	3.2	S	F			x
13	11/2/2012/21	12/2/2012/14	1.8	S	L	x	x	
14	12/2/2012/16	13/2/2012/02	0.9	S	L	x	x	x
15	14/2/2012/08	15/2/2012/14	2.8	S	U		x	
16	16/2/2012/10	16/2/2012/22	1.3	R/S	F	x	x	x
17	18/2/2012/10	18/2/2012/20	13.9	S	C		x	
18	20/2/2012/15	20/2/2012/17	0	None	Ri	x		
19	21/2/2012/18	22/2/2012/07	0.3	S	U	x		x
20	24/2/2012/11	25/2/2012/00	8.4	S	C	x	x	x

21	25/2/2012/01	25/2/2012/17	12.1	S	L	x
22	27/2/2012/20	28/2/2012/10	0.4	S	U	
23	29/2/2012/12	1/3/2012/10	12.7	S	C	
24	3/3/2012/01	3/3/2012/10	4.7	R	F	
25	4/3/2012/00	4/3/2012/13	1.5	S	F	

Figure 1: An overview of the experimental setting. Inset: Location in Ontario, Canada near the Great Lakes. The three aircraft (inset) were staged out of Bangor, Maine (DC-8), Muskoka, Ontario (UND Citation), and Ottawa, Ontario (Convair-580). The main ground site was the EC Centre for Atmospheric Research Experiments (CARE) with three additional sites within 15 km (Mortons to the west, Steamshow to the south, and Skydive to the east). A fourth site (Huronia) was located about 90 km to the north close to Georgian Bay. The EC dual polarization C-band radar (King City radar) is located about 34 km to south-southeast of CARE. The cities of Toronto and Barrie, Ontario, Canada are noted.

Figure 2: a) The project-long precipitation accumulation record for the manual DFIR measurements (black) and the Pluvio precipitation gauge (solid red). The dashed red line is the accumulation during the 25 events. The vertical shading indicates the events sampled with aircraft instruments (see Table 6); b) The derived 10 min averaged precipitation rates at CARE from the Pluvio gauge at CARE.

Figure 3: a) The project wide ground radar derived precipitation accumulation for January 30, 2012 in snow water equivalent. The numbers indicate the measured amounts of the 5 surface sites. The boxes indicate pre-defined flight zones. b) The time history of the accumulation at Huronia from the radar derived amounts (red) and the Pluvio gauge (black). The vertical shading indicates the project intensive observing events; yellow shading indicates the involvement of the research aircraft.

Figure 4: For the 27 January case: (a) Plan view of 2:32 UTC 0.8 degree King City C-band radar reflectivity PPI scan (dBZ), with the location of the CARE site and the DC-8 flight track overlaid. Panels (b-e) are from the DC-8 instrumentation centered at CARE at 2:30 UTC, matched along the radar cross sections in panels (a): (b) APR-2 Ku-band reflectivity (dBZ), (c) APR-2 Ku-Ka dual frequency ratio (DFR, dB), (d) CoSMIR cross-track scan brightness temperatures at the channels indicated in the legend, and (e) CoSMIR conical scan polarization difference at 89 GHz). In panels (b-e) the horizontal axis is distance in km from the CARE site along the track.

Figure 5: January 27 UND Citation aircraft spiral maneuver over CARE. Plotted including (a) Nevzorov Total Water Content measurement, (b) King probe liquid water content (black dot shows location of CARE facility, 44.23N -79.78W), and (c) Particle size distributions (m^{-3} mm^{-1}) measured by the combination of CIP and HVPS-3 probes (contoured) with calculation of mean diameter D_0 (pink line).

Figure 6: For the 30 January case: (a) Plan view of 0:31 UTC 0.8 degree King City C-band radar reflectivity PPI scan (dBZ), with the location of the CARE site and the DC-8 flight track overlaid. Panels (b-e) are from the DC-8 instrumentation from centered at CARE at 0:32 UTC, matched along the radar cross sections in panels (a): (b) APR-2 Ku-band reflectivity (dBZ), (c) APR-2 Ku-Ka dual frequency ratio (DFR, dB), (d) CoSMIR cross track scan brightness temperatures at the channels indicated in the legend, and (e) CoSMIR conical scan polarization

difference at 89 GHz. In panels (b-e) the horizontal axis is distance in km from the CARE site along the track.

Figure 7: As in Figure 5, but for the 30 January spiral. Note that the surface precipitation type is snow.

Figure 8: Crystal photographs taken by the University of Manitoba at 2330 30 January 2012 showing small (<3 mm diameter) irregular particles and aggregates at the surface. Note the scale at lower right; each box is 1 mm^2 in area.

Figure 9: For the 24 February 2012 case: (a) NMQ composite radar reflectivity, (b) DC-8 APR-2 Ku-band reflectivity, (c) Ku-Ka band dual frequency ratio, (d) CoSMIR cross-track brightness temperatures (T_b), and (e) CoSMIR 89 and 165 GHz polarization difference (V-H).

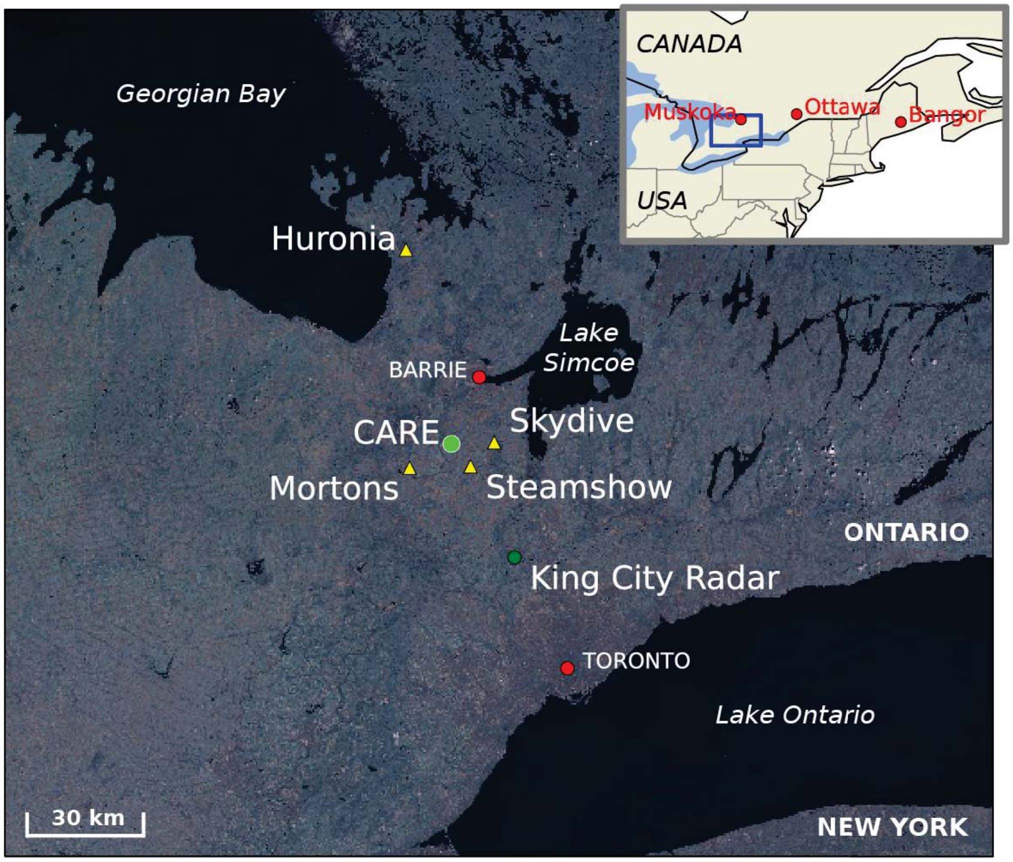

Figure 1: An overview of the experimental setting. Inset: Location in Ontario, Canada near the Great Lakes. The three aircraft (inset) were staged out of Bangor, Maine (DC-8), Muskoka, Ontario (UND Citation), and Ottawa, Ontario (Convair-580). The main ground site was the EC Centre for Atmospheric Research Experiments (CARE) with three additional sites within 15 km (Mortons to the west, Steamshow to the south, and Skydive to the east). A fourth site (Huronia) was located about 90 km to the north close to Georgian Bay. The EC dual polarization C-band radar (King City radar) is located about 34 km to south-southeast of CARE. The cities of Toronto and Barrie, Ontario, Canada are noted.

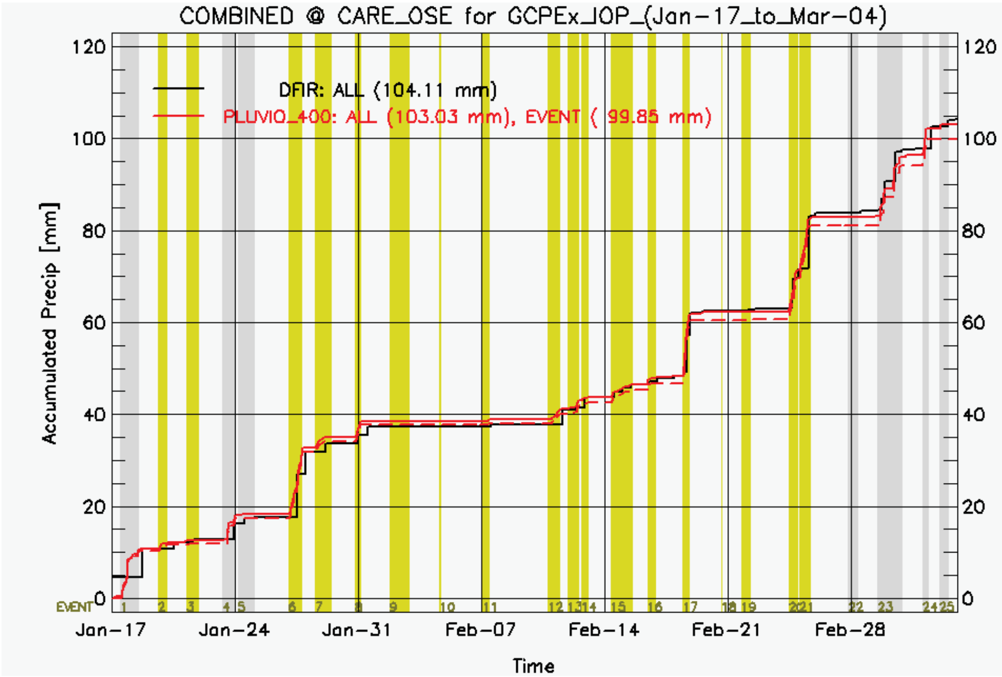

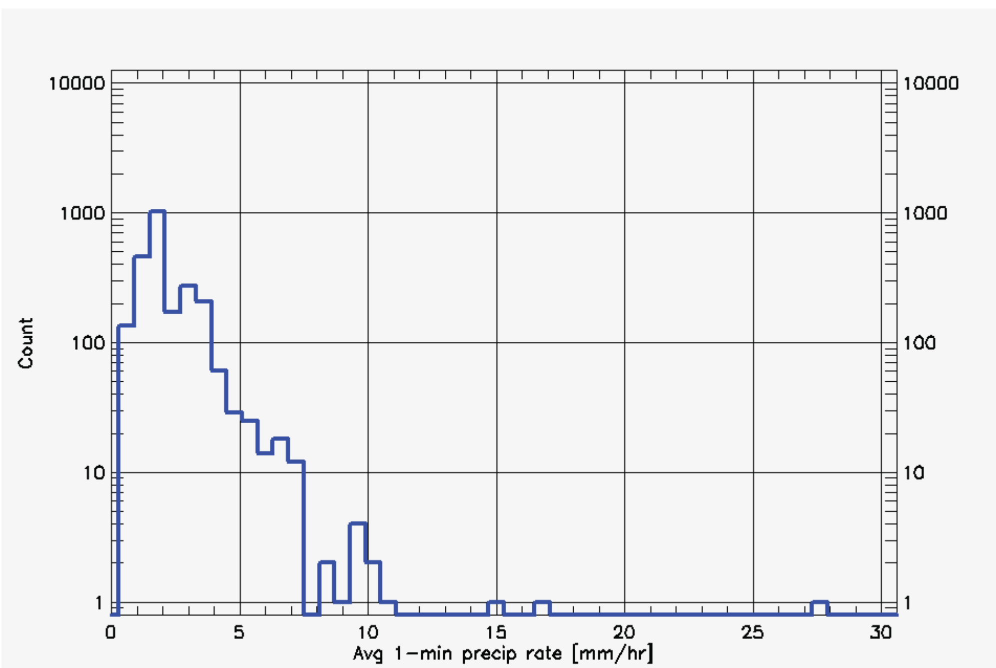

Figure 2: a) The project-long precipitation accumulation record for the manual DFIR measurements (black) and the Pluvio precipitation gauge (solid red). The dashed red line is the accumulation during the 25 events. The vertical shading indicates the events sampled with aircraft instruments (see Table 6); b) The derived 10 min averaged precipitation rates at CARE from the Pluvio gauge at CARE. The vertical shading indicates the project intensive observing events; yellow shading indicates the involvement of the research aircraft.

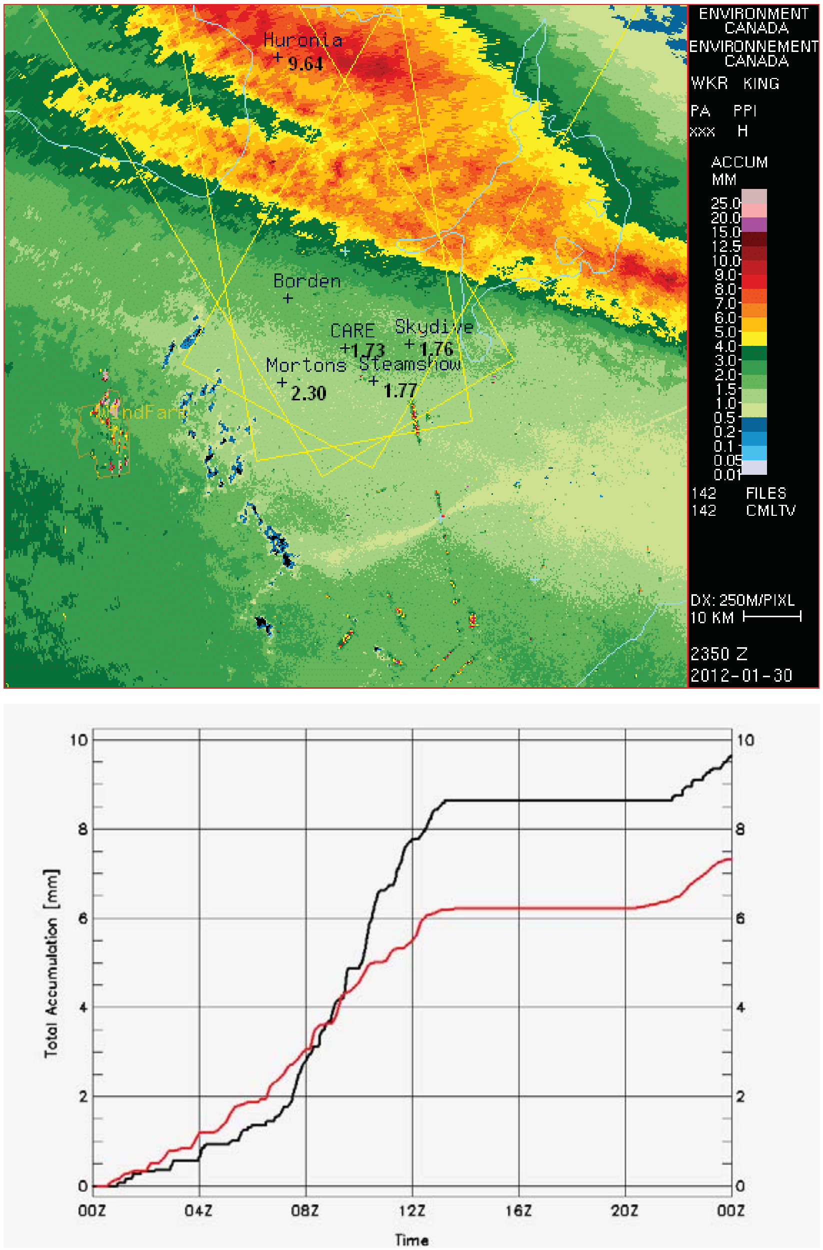

Figure 3: a) The project wide ground radar derived precipitation accumulation for January 30, 2012 in snow water equivalent. The numbers indicate the measured amounts of the 5 surface sites. The boxes indicate pre-defined flight zones. b) The time history of the accumulation at Huronia from the radar derived amounts (red) and the Pluvio gauge (black).

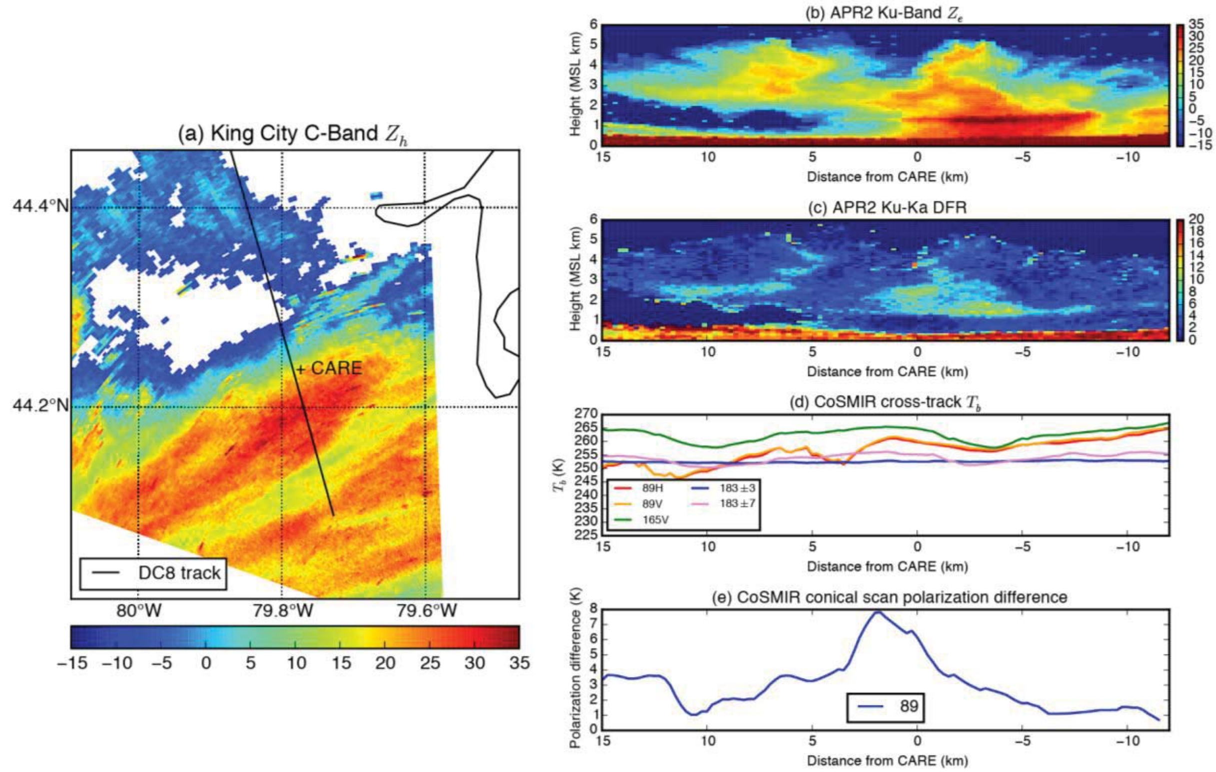

Figure 4: For the 27 January case: (a) Plan view of 2:32 UTC 0.8 degree King City C-band radar reflectivity PPI scan (dBZ), with the location of the CARE site and the DC-8 flight track overlaid. Panels (b-e) are from the DC-8 instrumentation centered at CARE at 2:30 UTC, matched along the radar cross sections in panels (a): (b) APR-2 Ku-band reflectivity (dBZ), (c) APR-2 Ku-Ka dual frequency ratio (DFR, dB), (d) CoSMIR cross-track scan brightness temperatures at the channels indicated in the legend, and (e) CoSMIR conical scan polarization difference at 89 GHz). In panels (b-e) the horizontal axis is distance in km from the CARE site along the track.

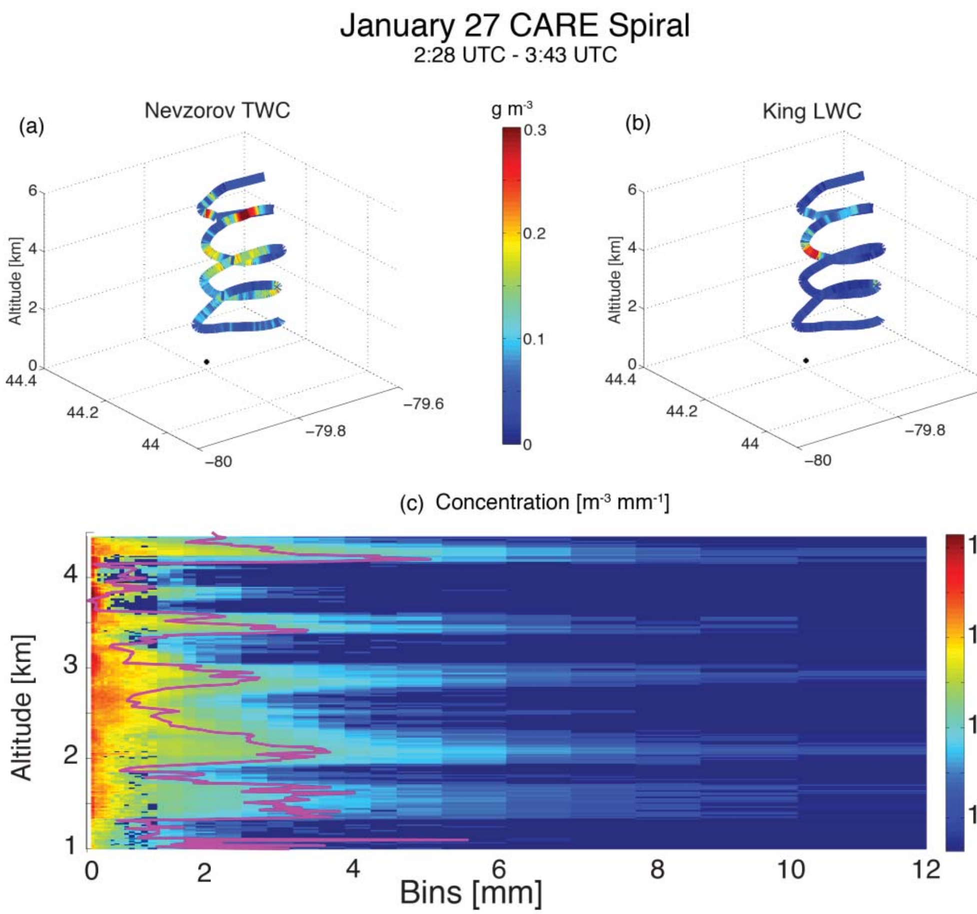

Figure 5: January 27 UND Citation aircraft spiral maneuver over CARE. Plotted including (a) Nevzorov Total Water Content measurement, (b) King probe liquid water content (black dot shows location of CARE facility, 44.23N -79.78W), and (c) Particle size distributions (m^{-3} mm^{-1}) measured by the combination of CIP and HVPS-3 probes (contoured) with calculation of mean diameter D_0 (pink line).

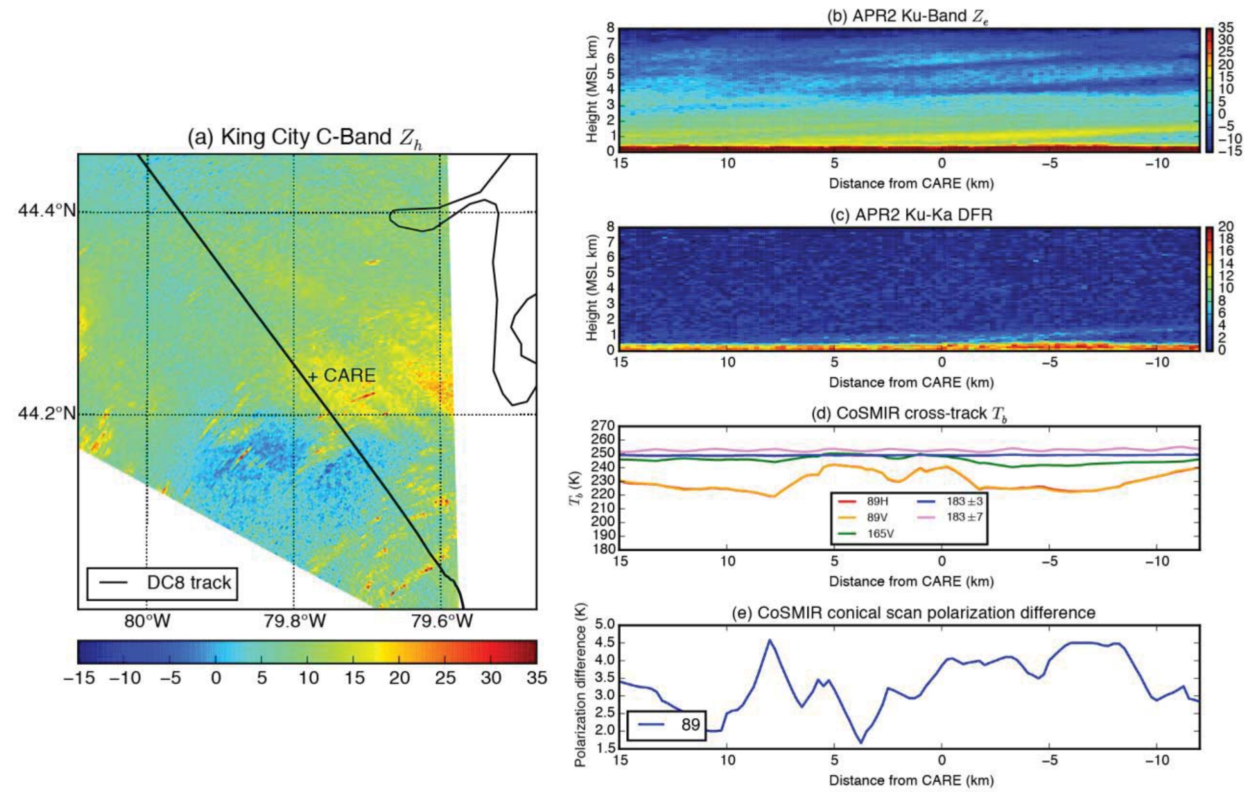

Figure 6: For the 30 January case: (a) Plan view of 0:31 UTC 0.8 degree King City C-band radar reflectivity PPI scan (dBZ), with the location of the CARE site and the DC-8 flight track overlaid. Panels (b-e) are from the DC-8 instrumentation from centered at CARE at 0:32 UTC, matched along the radar cross sections in panels (a): (b) APR-2 Ku-band reflectivity (dBZ), (c) APR-2 Ku-Ka dual frequency ratio (DFR, dB), (d) CoSMIR cross track scan brightness temperatures at the channels indicated in the legend, and (e) CoSMIR conical scan polarization difference at 89 GHz. In panels (b-e) the horizontal axis is distance in km from the CARE site along the track.

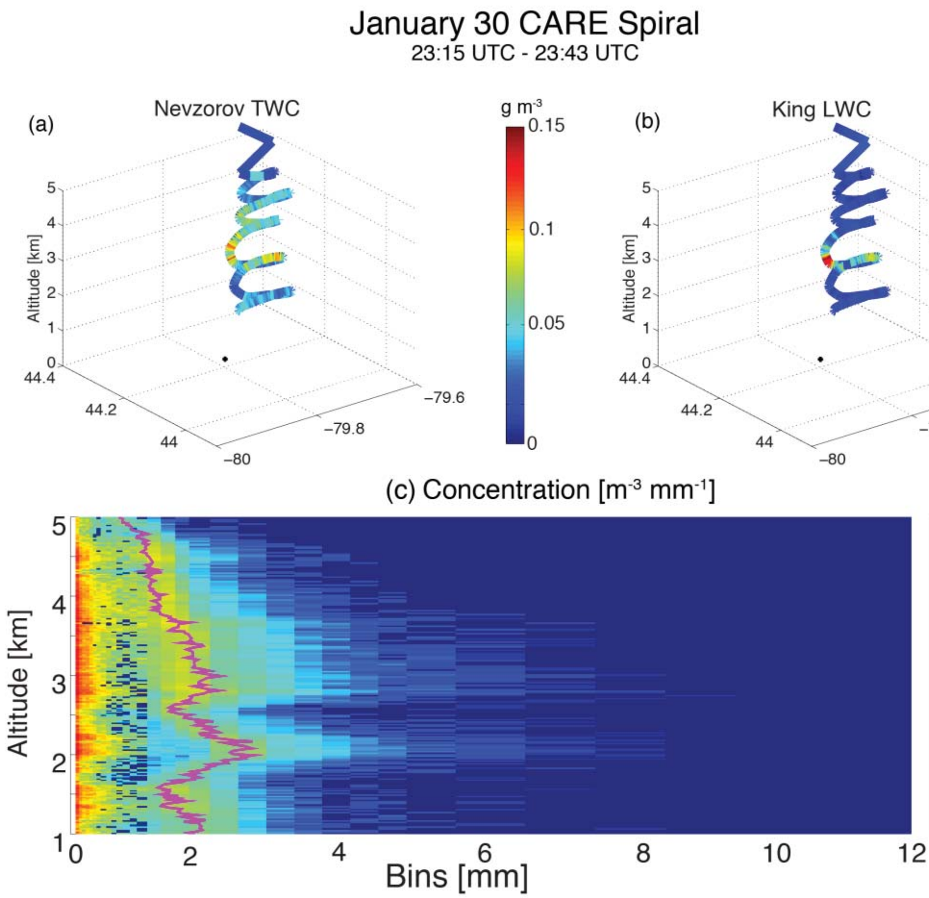

Figure 7: As in Figure 5, but for the 30 January spiral. Note that the surface precipitation type is snow.

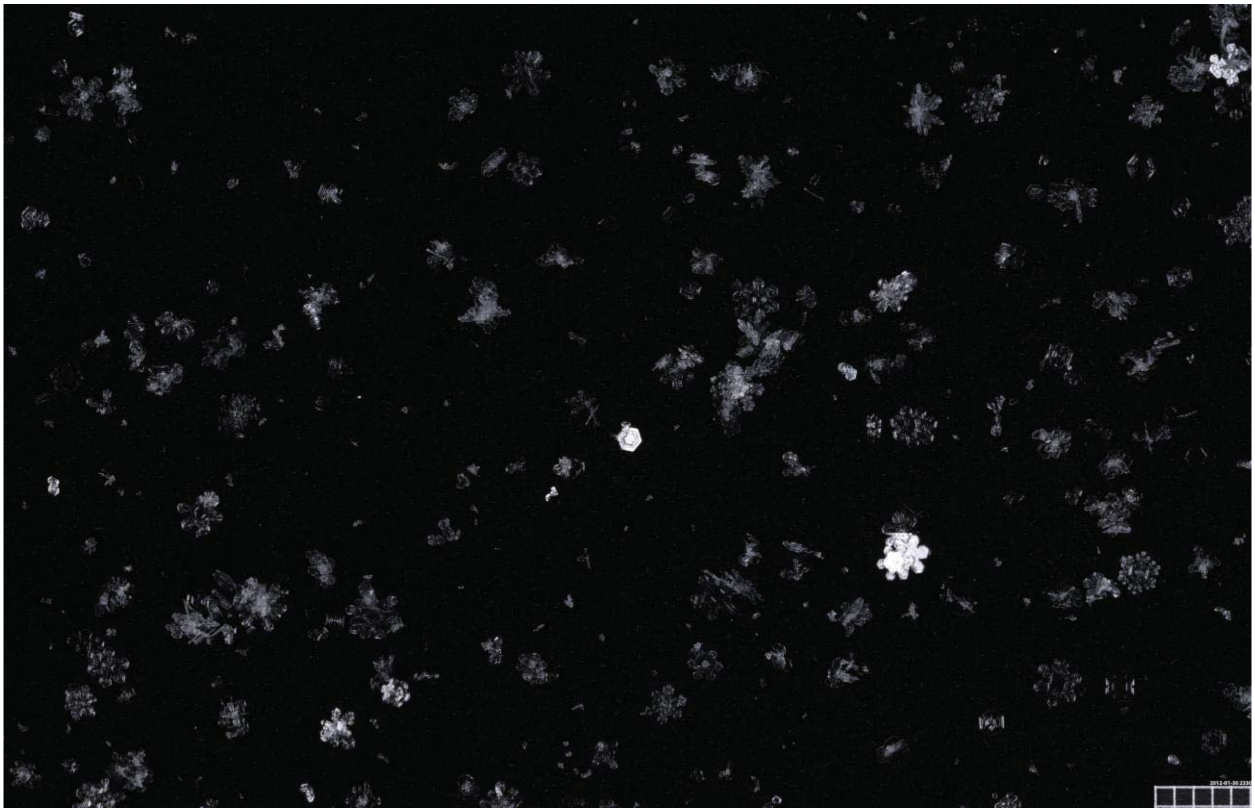

Figure 8: Crystal photographs taken by the University of Manitoba at 2330 30 January 2012 showing small (<3 mm diameter) irregular particles and aggregates at the surface. Note the scale at lower right; each box is 1 mm^2 in area.

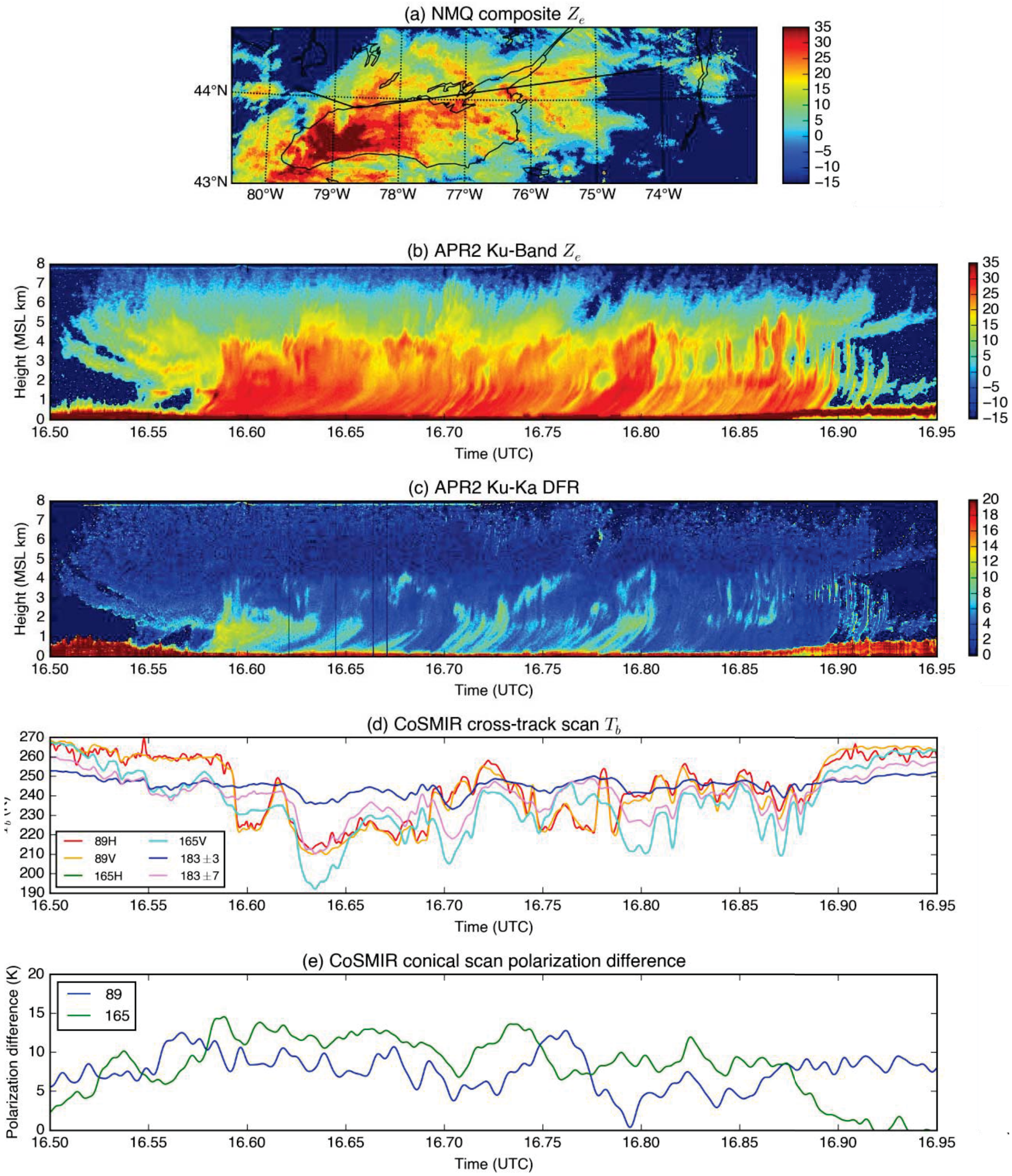

Figure 9: For the 24 February 2012 case: (a) NMQ composite radar reflectivity, (b) DC-8 APR-2 Ku-band reflectivity, (c) Ku-Ka band dual frequency ratio, (d) CoSMIR cross-track brightness temperatures (T_b), and (de) CoSMIR 89 and 165 GHz polarization difference (V-H).